Effects of CoFlow-Jet Active Flow Control on Airfoil Stall

Shima Yazdani
Quchan University of Technology
Erfan Salimipour
Quchan University of Technology https://orcid.org/0000-0003-2077-0566
Ayoob Salimipour
Quchan University of Technology
Mikhail Sheremet (sheremet@math.tsu.ru)
Tomsk State University
Mohammad Ghalambaz (mohammad.ghalambaz@tdtu.edu.vn)
Ton Duc Thang University

Original Article

Keywords: Active Flow Control, CoFlow-Jet (CFJ), Momentum Coefficient, Stall

Posted Date: March 28th, 2022

DOI: https://doi.org/10.21203/rs.3.rs-672095/v2

Effects of CoFlow-Jet Active Flow Control on Airfoil Stall

Shima Yazdani[1], Erfan Salimipour[1], Ayoob Salimipour[2], Mikhail Sheremet*[3], Mohammad Ghalambaz*[4,5]

[1]Department of Mechanical Engineering, Quchan University of Technology, Quchan, Iran

[2]Department of Mathematics, Quchan University of Technology, Quchan, Iran

[3]Department of Theoretical Mechanics, Tomsk State University, 36 Lenin Ave., Tomsk 634050, Russia

[4]Metamaterials for Mechanical, Biomechanical and Multiphysical Applications Research Group, Ton Duc Thang University, Ho Chi Minh City 758307, Vietnam; mohammad.ghalambaz@tdtu.edu.vn

[5]Faculty of Applied Sciences, Ton Duc Thang University, Ho Chi Minh City 758307, Vietnam

Contacts: shima.yazdaani@gmail.com (S. Yazdani); esalimipour@qiet.ac.ir (E. Salimipour); ayoob.salimipour@gmail.com (A. Salimipour); M. Sheremet (sheremet@math.tsu.ru); M. Ghalambaz (m.ghalambaz@gmail.com)

** Corresponding authors.*

Abstract

An active flow control method as CoFlow-Jet (CFJ) is implemented on the NACA 0024 airfoil at the chord-based Reynolds number of 1.5×10^5. For this purpose, an in-house solver based on the Reynolds averaged Navier-Stokes equations in two-dimensional, incompressible and unsteady form with the *SST-k-ω* turbulence model is prepared. Several levels of jet momentum coefficient (C_μ) are studied to achieve a proper momentum coefficient for each angle of attack (α). The findings demonstrate that at C_μ=0.06, the lift coefficients at low attack angles (up to α =15°) dramatically increase. Furthermore, the dynamic stall at the given Reynolds number and with the lowered frequency of 0.15 is explored. In the instance of C_μ=0.07, the lift coefficient curve does not show a noticeable stall feature compared to C_μ=0.05, suggesting that a more powerful stronger jet can entirely control the dynamic stall. The impact of raising the Reynolds numbers from 0.5×10^5 to 3×10^5 on this active flow control is also explored. The lift coefficient improves at all Reynolds numbers studied as C_μ increases, with the highest performance achieved at α = 15°.

Keywords Active Flow Control; Coflow-Jet (CFJ); Momentum Coefficient; Stall.

1. Introduction

Wind turbines convert the kinetic energy of the wind into electrical energy and are categorized into two types: vertical axis and horizontal axis. Generally, although horizontal-axis wind turbines (HAWT) are popular all around the world, they cannot be used in municipal areas, damage the environment, and need a high initial cost. Wind energy is considered as one the cheapest and most available renewable energy resources. However, due to different problems of HAWTs, wind turbines are not widely employed. Thus, vertical-axis wind turbines (VAWT) take on paramount importance (M. SaqibHameed and KamranAfaq, 2013). The most important superiority of this type of wind turbine is that they do not need to be adjusted relative to the wind direction. Regarding that the axis is vertical, the gearbox and generator can be installed near the ground, leading to maintenance and repair of these pieces of equipment. Since the blade tip is closer to the rotating axis in VAWTs, in comparison to HAWTs, they make lower noise. Furthermore, due to their smaller size, the peripheral collisions are reduced. NACA airfoils are designed for aircraft and wind turbines. Investigating airfoil characteristics, particularly in incompressible low-Reynolds flows, and changes in the aerodynamic performance of airfoils due to the amount of the Reynolds number is of paramount importance. Several investigations were conducted to study the performance of airfoils in the low Reynolds number region (Yarusevych et al., 2006b, Lissaman, 1983, Mueller and DeLaurier, 2003). Some studies indicated that serious aerodynamic problems might occur for below Reynolds number of about 500,000 (Yarusevych et al., 2006a, Srinath and Mittal, 2009, Salimipour, 2019a). The flow tendency through the airfoil's suction surface is to be separated in this Reynolds number range. On the other hand, the reverse pressure gradient that occurs in low Reynolds number airfoils causes the flow separation (Ok-Sok Gim and Lee, 2013). As the angle of attack increases, the vertical velocity and, consequently, the lift coefficient are

escalated. Furthermore, the drag coefficient is also enhanced since the vertical velocity depends on the air resistance. This trend continues up to a specific angle, called the stall angle. When stall happens, devastating effects on aerodynamic performance occur; the lift coefficient dramatically decreases while the drag coefficient increases (Salimipour and Yazdani, 2020, Abbasi and Yazdani, 2019). Thus, applying methods to control the stall phenomenon and the separation flow is important. The airfoil aerodynamic performance can be enhanced with the adequate energy and momentum transported to the boundary layer using flow control methods to reach desired aerodynamic goals, including delaying the transition, delaying the separation, and improving the aerodynamic efficiency. Many successful strategies have been developed (Velasco et al., 2017, Salimipour and Salimipour, 2019, Salimipour et al., 2021) to regulate flow separation and avoid the effects. In low Reynolds number aerodynamics, changing the shape of the airfoil is often employed to regulate separation and enhance the lift coefficient. Coflow-Jet (CFJ), is one of the active flow control approaches. The airfoil's suction surface features two slots in this technique: an injection slot near the leading edge and a suction slot near the trailing edge. In this flow control no mass adds to the system. Suction and injection in the airfoil surface, especially at high angles of attack, along with resistance to the reverse pressure gradient, connects the main flow and boosts boundary-layer velocity. Zha et al. (2006) in wind tunnel investigated the effects of injection slot size on the NACA 0025 at Reynolds number $Re = 3.8\times10^5$. Their research revealed that although a smaller injection slot size airfoil is better for boosting lift, a wider slot minimizes drag. Zha et al. (2007) studied the influence of the suction slot on efficiency numerically. For this purpose, two airfoils with the same injection slot (0.65% *c*) were studied with the suction slot equal to 1.96% *c* and the other without the suction slot. This study showed that the airfoil with the suction slot had better aerodynamic performances. For both airfoils compared to the baseline airfoil, the lift

coefficient increased, and the angle of attack was delayed. The airfoil without a suction slot, the stall occurred at 39°, and the other until 43° the stall did not happen. Zha and Gao (2006) experimentally performed the effects of the CFJ on the NACA 0025 at Reynolds 3.8×10^5. They looked at various pressure ratios and found that the lift coefficient rose by 220% compared to the baseline in the jet case. They also numerically performed their experimental results, and there was a good agreement between the data for the lift coefficient. However, the angle of attack of the stall was forecasted in numerical results three degrees more than experiments. The effects of adjusting the injection slot size on the lift coefficient, stall angle, and drag coefficient were explored experimentally by Wells et al. (2006). Their findings revealed that an airfoil with a smaller injection slot would need less energy to attain the same lift coefficient as one with a bigger injection slot. Chng et al. (2009) experimentally investigated the jet concept's performance on a Clark-Y airfoil. Furthermore, they compared the aerodynamic performance of the synchronous suction and injection, pure injection, and pure suction. Their findings demonstrated that the simultaneous suction and injection mechanism is more effective than pure injection and pure suction. Abinav et al. (2016), using Ansys Fluent, compared the performance of the NACA 6409 baseline airfoil and the three jet airfoils with different injection and suction slot locations. The influence of jet on the S809 airfoil was numerically examined by Xu et al. (2015) at three jet momentum coefficient values. According to their findings, the jet greatly reduces the drag coefficient and positively influences lift and stall margin. Ethiraj (2017) examined the impact of jet mathematically, and his results for a 12° angle of the attack suggest a 25-30% decrease in drag and a 10-20% increase in lift coefficient. Siddanathi (2016) used a jet on NACA 652-415 airfoil to investigate this active flow control on increasing the lift. Lefebvre and Zha (2013) numerically studied the effect of jet flow control on a pitching airfoil at the Reynolds number of 3.93×106 and

reduced frequency between 0.05 and 0.2. Moreover, Xu et al. (2016) simulated the dynamic stall phenomenon for a wind turbine blade using the jet. Khoshnevis et al. (2020) examined the effects of jets on symmetric NACA airfoils in transitional flow, considering thickness variation. In another investigation, they analyzed the influence of this flow control on NACA 0025 at different Reynolds numbers (Khoshnevis et al., 2020).

In the present paper, active flow control on the NACA 0024 airfoil defined as suction-injection jet (CFJ) at the chord-based Reynolds number of 1.5×10^5 is studied. The two-dimensional incompressible unsteady Reynolds-Averaged Navier-Stokes equations with the *SST* k-ω turbulence model are utilized to study the effects of CFJ on the dynamic and static stall phenomena. CFJ implementation is conducted with several momentum coefficients to investigate their turnover. Furthermore, the current work intends to analyze the CFJ performance by varying the Reynolds number and jet momentum coefficient and comparing all states to the baseline airfoil, which has not been studied in prior research investigations.

2. Model Description

The CFJ is constructed at the suction surface of the baseline NACA 0024 airfoil to produce a jet tangential to the main flow; the heights of an injection slot and a suction slot are considered 0.006 and 0.019 times the chord length, respectively. The suction and injection slots are located at distances of 0.83 and 0.07 times the chord length from the leading edge. Based on the considered geometry, various meshing strategies can be employed where we choose a “C” grid to solve the flow using the elliptic method. Fig. 1 shows a close-up view of this grid together with the situation of the CFJ on the airfoil. The nodes have an adequate perpendicular to one another, as can be shown.

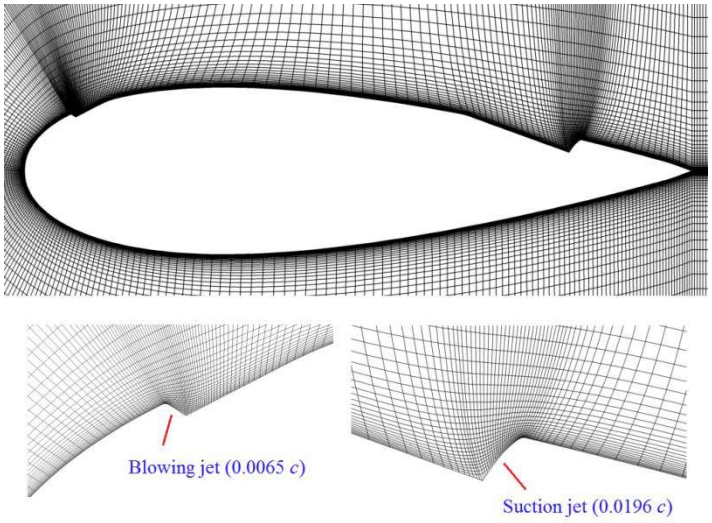

Fig. 1. The grid used in flow computations and situation of the CFJ on the airfoil.

Fig. 2 shows the solution domain and boundary conditions. The velocity inlet boundary includes a constant value of U_∞ for the horizontal velocity component, zero for the vertical velocity component, and a zero normal gradient for the pressure (Ghalambaz et al., 2020). On the pressure outlet boundary, a fixed value of p_∞ is applied for the pressure, and the normal gradient of the velocities is assigned to zero. On the solid wall, a no-slip boundary condition is considered.

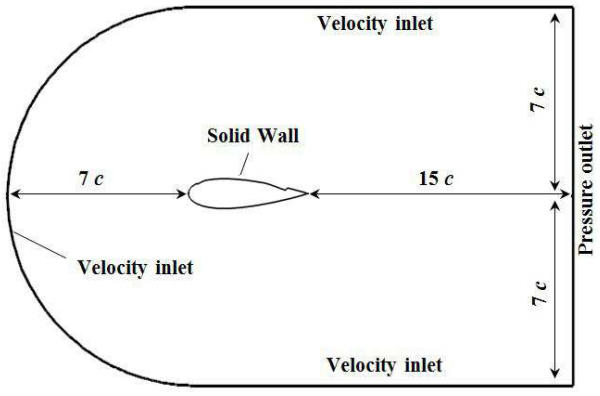

Fig. 2. Boundary conditions around the NACA 0024 airfoil.

3. Mathematical and Numerical Formulation

The integral formulations of the Reynolds-averaged Navier-Stokes equations, which include continuity and momentum, are as follows (Salimipour, 2019b):

$$\oint_{\partial\Omega} \rho V \, dS = 0 \tag{1}$$

$$\frac{\partial}{\partial t}\int_{\Omega} \vec{W} \, d\Omega + \oint_{\partial\Omega} \vec{J} \, dS = 0 \tag{2}$$

where ρ denotes the density, Ω is a volume surrounded by the control surface $\partial\Omega$, V is the velocity perpendicular to the surface element dS, $\vec{W}$ represents the conservative variables vector, and $\vec{J}$ consists of the convective and diffusive fluxes which can be written as follows (Salimipour, 2019a):

$$\vec{W} = \begin{bmatrix} \rho u \\ \rho v \end{bmatrix}, \quad \vec{J} = \begin{bmatrix} \rho u V + n_x p - (\mu + \mu_t)\left(n_x \frac{\partial u}{\partial x} + n_y \frac{\partial u}{\partial y}\right) \\ \rho v V + n_y p - (\mu + \mu_t)\left(n_x \frac{\partial v}{\partial x} + n_y \frac{\partial v}{\partial y}\right) \end{bmatrix}, \tag{3}$$

$$V \equiv \vec{v}.\vec{n} = n_x u + n_y v \tag{4}$$

where μ and μ_t denote the laminar and turbulent viscosity, respectively. The flow equations (1) and (2) are solved by a pressure-based method proposed by Rajagopalan and Lestari (2016). The momentum equation is discretized with second-order precision in time and space (Stone, 1968). To simulate the turbulent viscosity (μ_t), the *SST k-ω* turbulence model is used. The flow variables are normalized as expressed in (Hashem Zadeh et al., 2020). The flow parameters required, such as velocity and pressure components, streamlines, and drag and lift coefficients, could be obtained by numerically solving the previously given equations. The jet momentum coefficient C_μ is a parameter that is used to determine the strength of the jet. It is as follows (Bak Khoshnevis et al., 2020):

$$C_\mu = \frac{\dot{m}U_j}{{}^1/_2\rho_\infty U_\infty^2 c} \quad (5)$$

where U_j and $\dot{m}$ denote the velocity and mass flow of injection; U_∞ and ρ_∞ are the free stream velocity and density; and c is the airfoil chord length. For cases with a CFJ on, the overall aerodynamic force is estimated according to the analysis in (Zha et al., 2007, Xu et al., 2015). The following is an expression for the overall lift and drag coefficients:

$$C_l = C_{l,pressure} + C_{l,stress} + C_{l,jet} \quad (6)$$

$$C_d = C_{d,pressure} + C_{d,stress} + C_{d,jet} \quad (7)$$

where subscripts *pressure*, *stress* and *jet* indicate the pressure force, frictional force and jet mass flow thrust, respectively. $C_{l,pressure+stress}$, and $C_{d,pressure+stress}$ be computed using the solver's standard integral approach, while $C_{l,jet}$, $C_{d,jet}$ are achieved using relations as follows:

$$C_{l,jet} = \frac{\dot{m}_j(\vec{V}_{j1} - \vec{V}_{j2})\vec{j}}{{}^1/_2\rho_\infty U_\infty^2 c} \quad (8)$$

$$C_{d,jet} = \frac{\dot{m}_j(\vec{V}_{j1} - \vec{V}_{j2})\vec{i}}{{}^1/_2\rho_\infty U_\infty^2 c} \quad (9)$$

where ($\vec{i}$, $\vec{j}$) is the unit vector indicating the lift and drag direction and $\vec{V}_{j1}$, $\vec{V}_{j2}$ are velocity vectors of the jet at injection and suction slots, respectively.

The pitching motion of the airfoil for dynamic stall analysis is described by the following equation:

$$\alpha(t) = 10^o + 10^o sin(2k\tau) \quad (10)$$

where $k = \omega c / 2U_\infty$ is the reduced frequency and $\tau = tU_\infty / c$ denotes the non-dimensional time. For quantifying the improvement of results from CFJ to enhance lift and decrease drag coefficients for the dynamic stall study, the differences in the area under the C_l and C_d curves between control cases and the baseline airfoil are calculated. This is accomplished as follows (where q is either lift or drag):

$$\Delta A_{C_q} = \frac{\int_0^{2\pi}\left(C_q^{baseline} - C_q^{CFJ}\right) d\varphi}{\int_0^{2\pi} C_q^{baseline}\, d\varphi} \tag{11}$$

where φ denotes the phase angle of the pitching motion in radians. In order to compare the results of the CFJ case with the baseline airfoil, three performance parameters are used defined as follows:

$$\eta(C_l) = \left|\frac{C_{l_{CFJ}} - C_{l_{Baseine}}}{C_{l_{Baseine}}}\right| \times 100 \tag{12}$$

$$\eta(C_d) = \left|\frac{C_{d_{CFJ}} - C_{d_{Baseine}}}{C_{d_{Baseine}}}\right| \times 100 \tag{13}$$

$$\eta(C_l/C_d) = \left|\frac{C_l/C_{d_{CFJ}} - C_l/C_{d_{Baseine}}}{C_l/C_{d_{Baseine}}}\right| \times 100 \tag{14}$$

4. Results and Discussion

4.1. Grid resolution study

Meshes with varying numbers of cells were assessed, and their results were compared to explore the grid independency of the solution domain. Three grids of 25000, 30000, and 38000 cells were investigated, as shown in Fig. 3. This comparison of pressure coefficients of the CFJ by the mentioned grids was performed at Re = 1.5×10^5, $\alpha = 15^o$, and $C_\mu = 0.13$. The results for 30000 and 38000 cells were very similar. This study selected the grid with N = 38000 cells for the conducted computations.

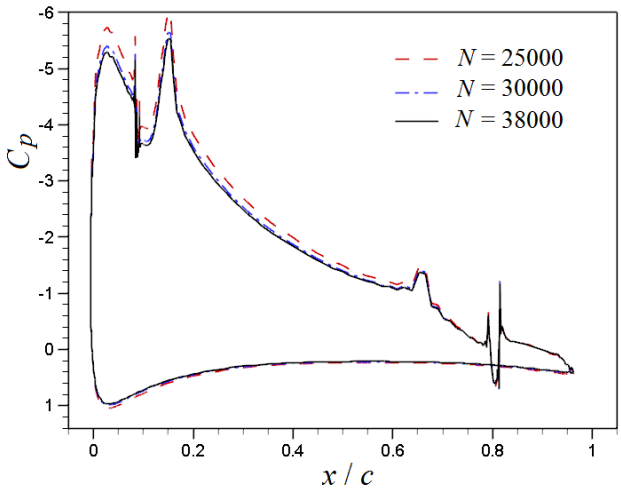

Fig. 3. Comparison of pressure coefficients of CFJ airfoil with different computational grids at Re = 1.5×10^5, α = 15° and C_μ = 0.13.

4.2.Code validation research

It is vital to assess the flow solver's validity before utilizing the developed code and validating its correctness. Experimental data obtained by Zha et al. (2006) used experimental data to assess solver capabilities for the configuration of NACA 0025 at Reynolds number of 3.8×10^5. Fig. 4 compares the lift to drag ratio of the current solution to experimental data. The prognostications are in nearby conjunction with the experimental data (Zha et al., 2006).

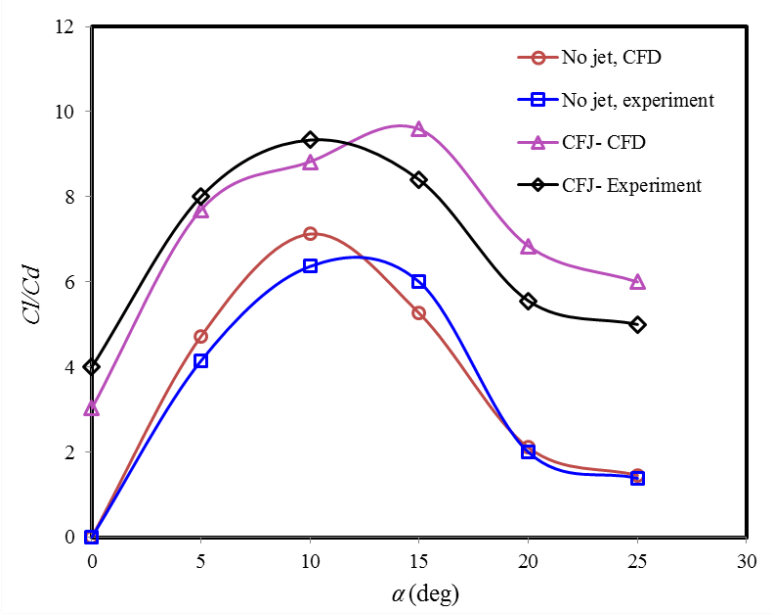

Fig. 4. Comparison of C_l/C_d between the current solver and the data from experiments (Zha et al., 2006).

4.3. Effect of momentum coefficient of CFJ on static stall at Re = 1.5×10^5

In this study, several momentum coefficients (C_μ) for the angles of attack in the range of 0 - 30 degrees at Re = 1.5×10^5 on the NACA 0024 airfoil are investigated to understand which momentum coefficient has an agreeable act at each attack angle. Fig. 5 shows the pressure coefficients' streamlines and contours for the baseline geometry at the angles of attack α = 5°, 10°, 13°, and 15°. The growth and shedding of the vortices can be seen for $\alpha \geq 10°$.

Fig. 6 shows the streamlines around the CFJ airfoil with C_μ = 0.05 at α = 15°. By applying the CFJ, the vortices on the airfoil are removed. The CFJ injects momentum into the boundary layer, resisting the flow separation because of the adverse pressure gradient.

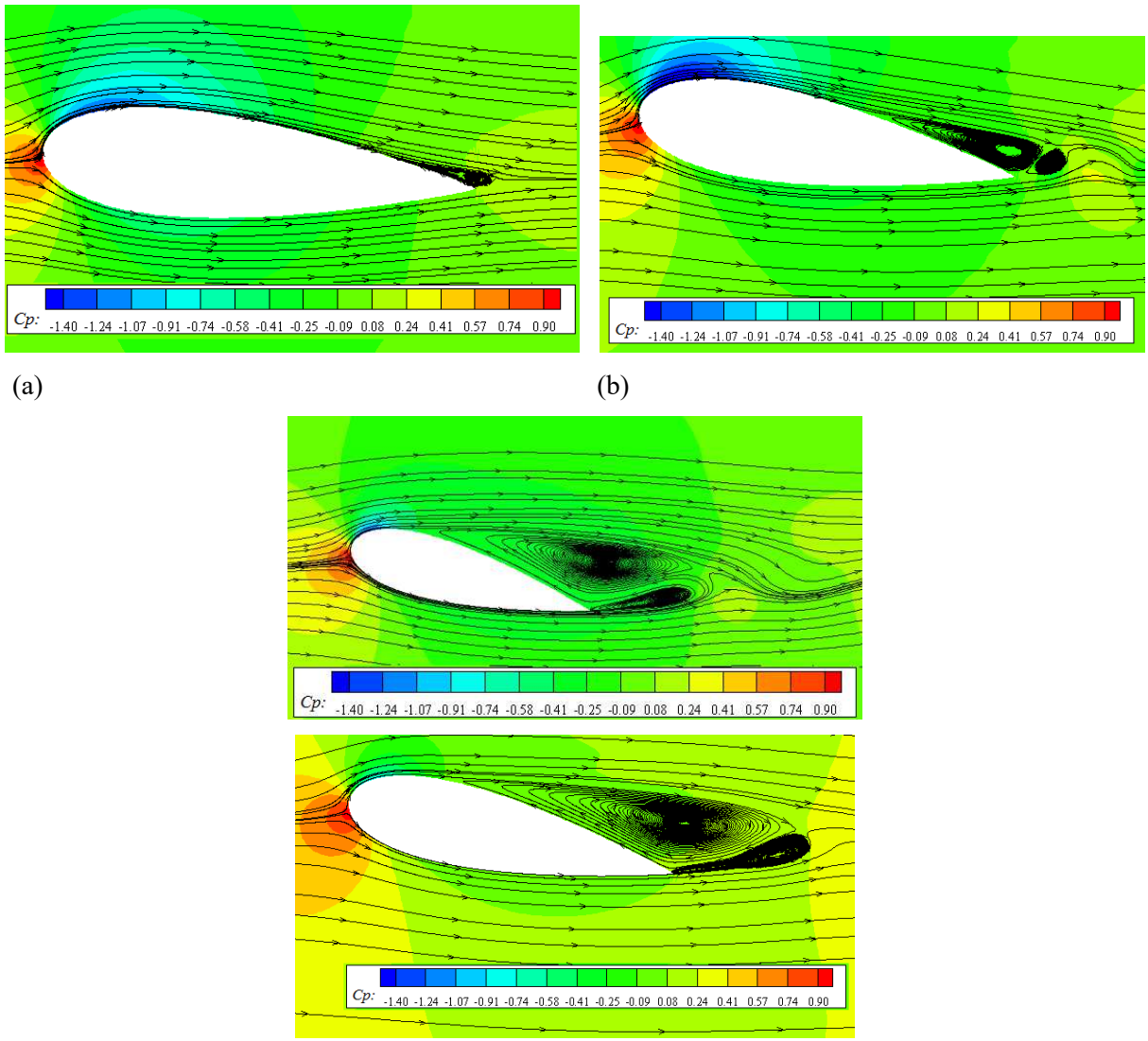

Fig. 5. Streamlines and pressure coefficient contours at several attack angles for baseline geometry, (a) α =5˚, (b) α = 10˚, (c) α =13˚, (d) α=15˚.

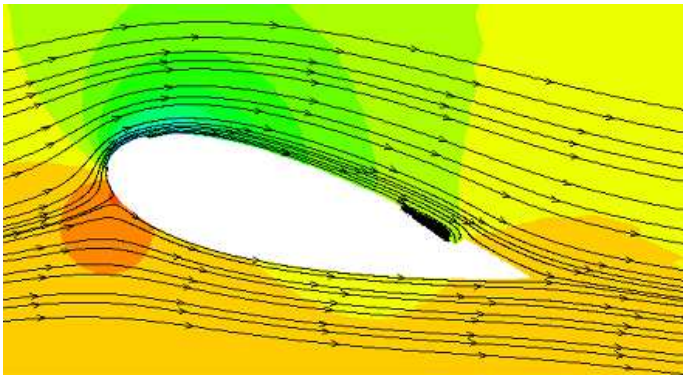

Fig. 6. Streamlines and pressure coefficient contours for CFJ geometry at α = 15˚and C_μ = 0.05.

Fig. 7 shows the pressure coefficient distributions of the baseline and CFJ airfoils at α=15˚and C_μ = 0.05 - 0.13. The spikes in the plots are due to the jet inlet and outlets. The comparisons demonstrate that the suction peak around the leading edge of the CFJ airfoils is much greater than that of the baseline airfoil. This effect causes the airfoil's lift to rise while decreasing its pressure drag. The pressure coefficient has a maximum absolute value of 5.6 at C_μ=0.13, whereas the baseline airfoil has a value of 1.5. The temporal fluctuations of the lift coefficients for baseline and CFJ airfoils with varying momentum coefficients α = 15˚are shown in Fig. 8.

It can be seen that all the curves finally become unchanged over time, and thus, the flow at this angle of attack has been steady. Furthermore, the baseline airfoil curve trend indicates that the stall occurs at this angle of attack, unlike the other curves.

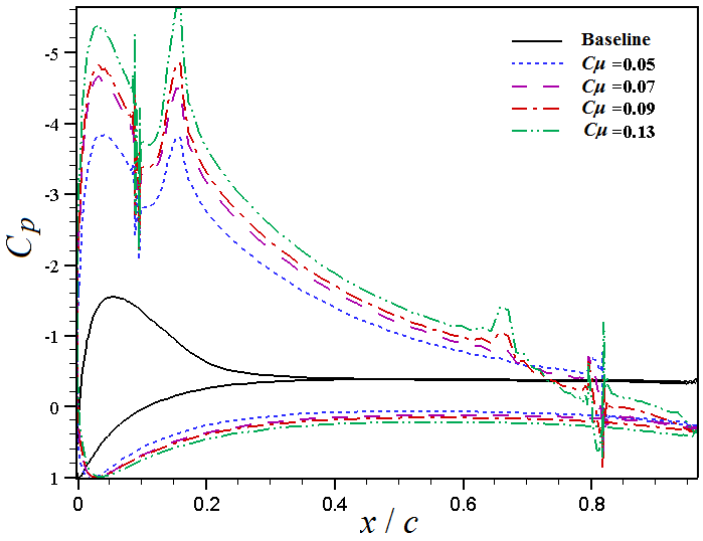

Fig. 7. Comparison of the pressure coefficient distributions at α = 15˚for various C_μ levels.

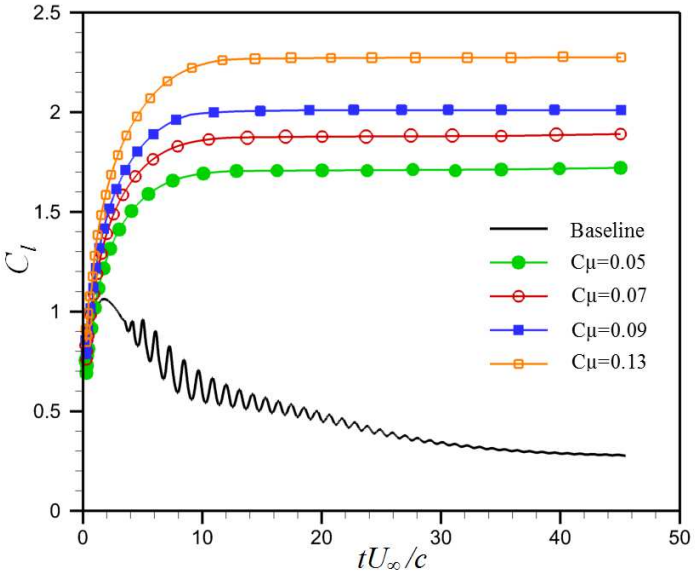

Fig. 8. Temporal variations of lift coefficients at $\alpha = 15^\circ$ for different C_μ levels.

The lift to drag ratio is an essential statistic for aircraft aerodynamic performance. Fig. 9 depicts the lift to drag coefficient curves for various momentum coefficients with respect to the angle of attack. The CFJ airfoils, compared to the baseline airfoil, have a dramatic gain in the lift to drag coefficients and cause the stall to occur at the higher angles of attack maintained with higher values of C_μ. As observed, increasing the momentum coefficient increases the stall angles and maximum lift to drag coefficients for all CFJ airfoils. The lift to drag coefficient diagram shows that for the CFJ airfoil with C_μ = 0.05, there is a significant increase for the C_l / C_d, and the stall angle is delayed compared to the baseline airfoil. At C_μ = 0.06 and $\alpha \leq 15°$, the highest C_l / C_d is observed. As the angle of attack increases from α = 20° to 30°, the C_l / C_d decreases. At C_μ = 0.13 and $\alpha \leq$ 10°, the use of CFJ is not affordable, while for $\alpha \geq 15°$, a significant C_l / C_d is obtained because of the significant lift generation. For the other angles, the maximum C_l/C_d is distinct at each angle of attack. The baseline airfoil result shows the stall occurrence around α = 10°, whereas for the CFJ airfoils results with C_μ = 0.05 - 0.07, the stall occurs at α =15°. With further increase in the

momentum coefficients, the stall angles increase, and at C_μ = 0.13, the stall does not occur up to α =30°. Fig. 10 shows the stall angles versus the different momentum coefficients. A sharp slope is observed from C_μ = 0.09 to 0.13.

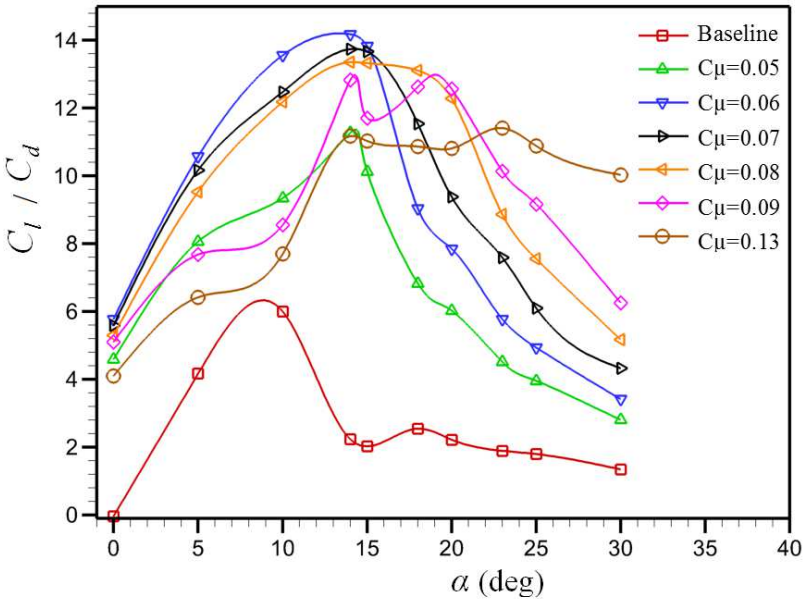

Fig. 9. Comparison of lift to drag coefficients for different C_μ levels.

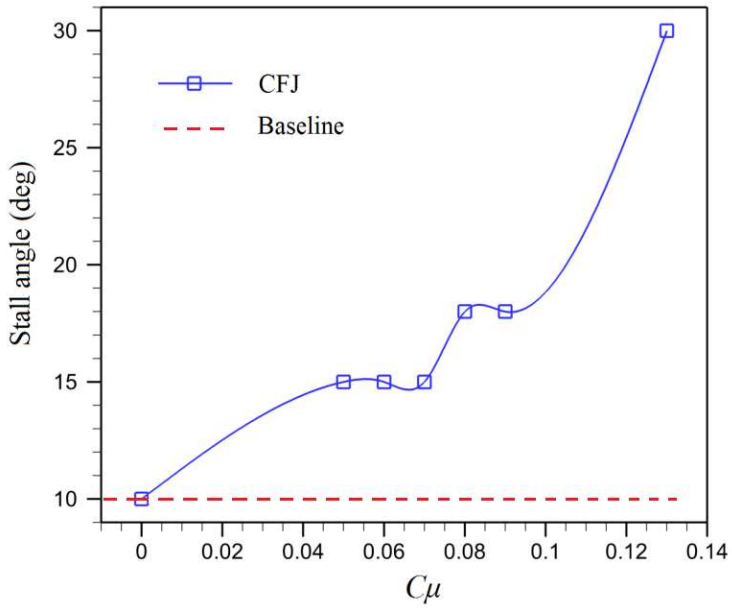

Fig. 10. Variation of stall angles for different C_μ levels.

Fig. 11 shows the optimum C_μ corresponding to $(C_l/C_d)_{max}$ for different angles of attack. Within the range of 15°< α <23°, by increasing the momentum coefficient, the lift to the drag ratio is enhanced, increasing the energy consumption of the CFJ. It can also be seen that the CFJ has the highest lift ratio to the drag at 14°. It should be noted that the required momentum coefficient at this angle compared to other angels has the smallest value. Fig. 12a and 12b show the velocity profiles for the baseline and CFJ cases with the momentum coefficients C_μ = 0.05 and 0.09 at x/c = 0.3 and 0.6, respectively. In both sections, the boundary-layer momentum of the CFJ cases is significantly increased compared to the baseline airfoil.

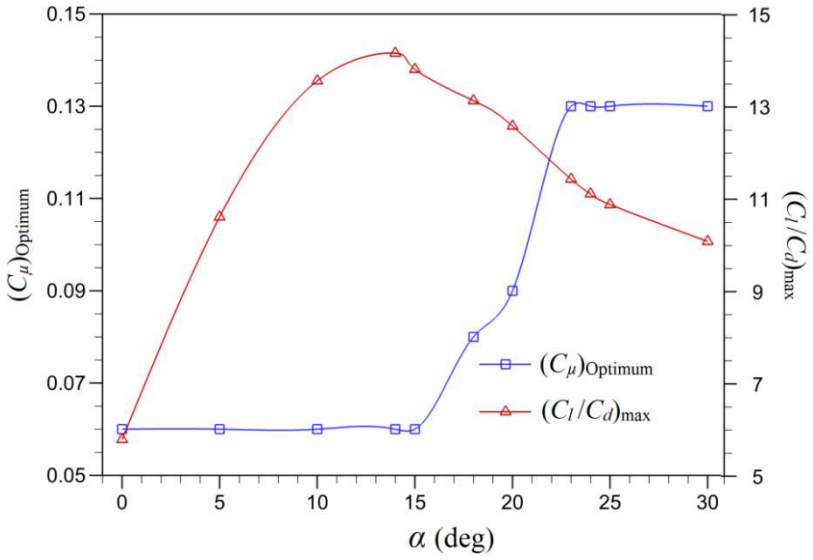

Fig. 11. Optimum C_μ and maximum C_l/C_d for different Angles of attack.

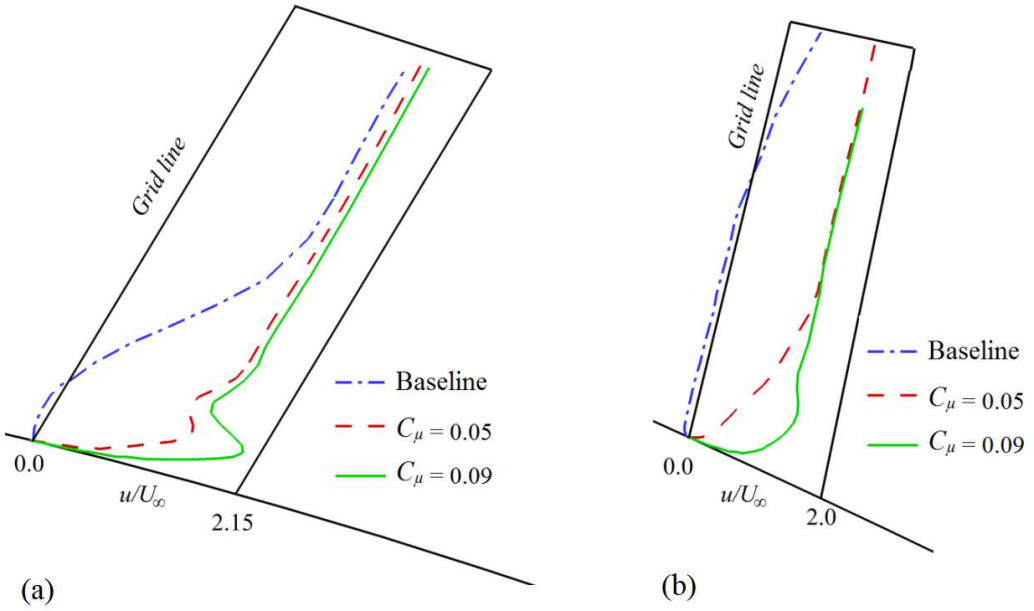

Fig. 12. Comparison of velocity profiles near the airfoil surface at α=15˚, (a) x/c=0.3, (b) x/c=0.6.

Table 1 shows the comparison of the maximum lift coefficients and locations of the stall onset between the baseline and CFJ cases. The CFJ significantly increases the maximum lift.

Table 1. Comparison of maximum lift coefficients and locations of stall onset.

Cases	Maximum C_l	Stall angle (deg.)	Increment in $C_{l\,max}$ relative to the baseline (%)	Increment in stall angle relative to the baseline (deg.)
Baseline	0.6	10	---	---
$C_\mu = 0.05$	1.26	15	110.00%	5
$C_\mu = 0.06$	1.76	15	193.33%	5
$C_\mu = 0.07$	1.9	15	216.67%	5
$C_\mu = 0.08$	2.16	18	260.00%	8
$C_\mu = 0.09$	2.25	18	275.00%	8
$C_\mu = 0.13$	3.11	30	418.33%	20

4.4. Effect of CFJ on the dynamic stall at Re = 1.5×10^5

Another investigation in this paper is about the influence of CFJ on the dynamic stall phenomena. The simulation is performed at $k = 0.15$ for the baseline airfoil and two CFJ cases with $C_\mu = 0.05$ and 0.07. By increasing the momentum coefficient, more energy can be transferred into the boundary layer; consequently, the lift coefficient is increased. Fig. 13 shows the lift coefficient curve for the CFJ control cases and the baseline airfoil. As can be seen, the lift coefficient curve for the CFJ case with $C_\mu = 0.05$ shifts up and is increased, compared to the baseline airfoil; however, the stall still occurs and this behavior is almost similar to the baseline airfoil. As expected, raising the momentum coefficient from 0.05 to 0.07 reduces the lift coefficient hysteresis loop.

Furthermore, in the case of $C_\mu = 0.07$, the lift coefficient curve lacks the stall feature, indicating that a more powerful jet may fully control the dynamic stall. The maximum lift coefficient for the baseline airfoil is equal to 1.15 and for the CFJ cases for $C_\mu = 0.05$ and 0.07 is equivalent to 2.06 and 2.16, respectively. Regarding the drag curves, Fig. 14 shows the CFJ control cases with $C_\mu = 0.05$ and 0.07 and the baseline airfoil. The maximum drag coefficient for the baseline airfoil and two CFJ cases is 0.54, 0.32, and 0.21. Therefore, for the case with $C_\mu = 0.07$, the maximum drag coefficient is decreased by 61%; furthermore, its hysteresis loop becomes smaller and smoother.

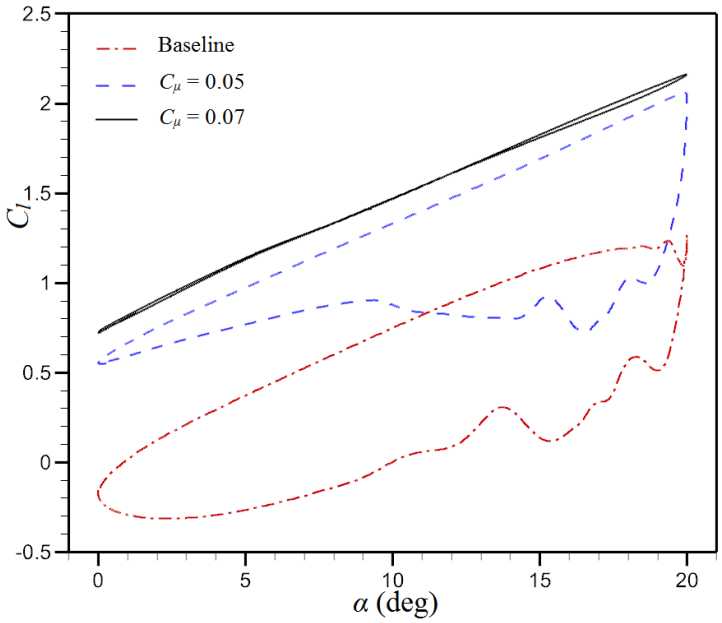

Fig. 13. Lift coefficient comparison between the CFJ and baseline airfoils.

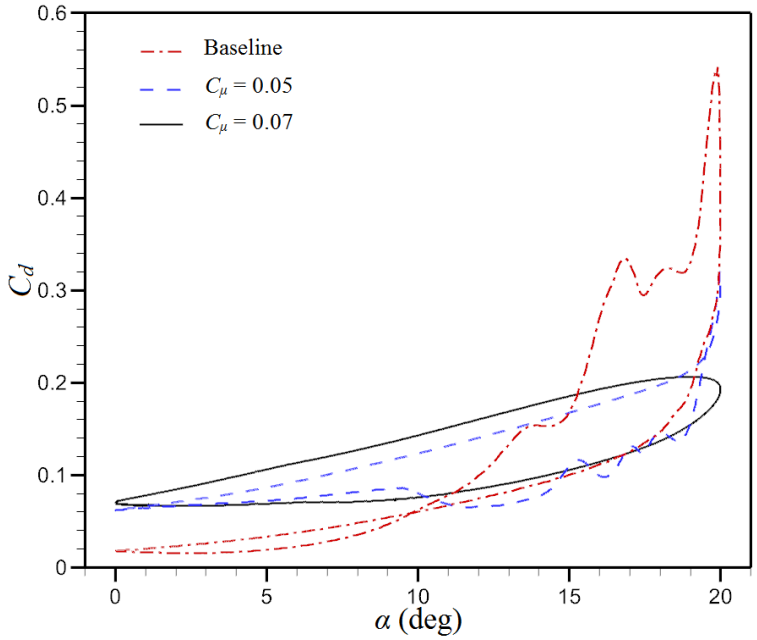

Fig. 14. Drag coefficient comparison between the CFJ and baseline airfoils.

Table 2 presents the averages of the aerodynamic hysteresis loops for two cases with $C_\mu = 0.05$ and 0.07. In order to quantify the enhancement in the lift and the reduction in the drag coefficients

over a pitch cycle due to CFJ cases, the differences within the area under the C_l and C_d curves between the control and baseline cases are computed. The resulting values due to the CFJ control are summarized in Table 2. It is discovered that by adopting the CFJ, the average lift coefficient can be greatly raised, and the average drag coefficient can also be somewhat raised. Finally, the results at C_μ = 0.07 show that the relative difference of the lift and drag coefficients (ΔA_{C_l}, ΔA_{C_d}) are improved compared to the baseline airfoil.

Table2. Effects of CFJ control compared to the baseline (k = 0.15).

coefficient	Baseline	c_μ = 0.05	c_μ = 0.07
$C_{l,\,ave}$	0.36	1.08	1.44
$C_{d,\,ave}$	0.099	0.11	0.115
$C_{l,\,ave}/\,C_{d,\,ave}$	3.64	9.82	12.52
ΔA_{C_l}	-	200%↑	300%↑
ΔA_{C_d}	-	12%↑	16%↓

4.5. Reynolds number effects

The influence of the CFJ method on the aerodynamic performance of the airfoil is studied at five Reynolds numbers from 0.5×10^5 to 3×10^5. This evaluation is carried out for different jet momentum coefficients of 0.03, 0.06, 0.09, and 0.13 in a range of angle of attack from 0° to 20°. Fig. 15 depicts the performance of the lift coefficient for the CFJ airfoil in comparison with the baseline airfoil at different Reynolds numbers and momentum coefficients. The present results indicate that at these Reynolds numbers, use of flow control is of more importance than that for other cases where its results have the best performance among all angles of attack at different momentum coefficients. Furthermore, at all investigated Reynolds numbers, the angle of 15° offers the best performance of lift coefficient for the CFJ airfoil compared to the baseline airfoil. The

stall occurs at lower angles of attack for the baseline airfoil while it is delayed for the CFJ airfoil. This is the reason for the improvement of airfoil performance regarding the lift coefficient at the angle of 15°. In the baseline airfoil, the lift coefficient is reduced after the occurrence of the stall phenomenon that can be seen at the angle of 15°, while by applying the CFJ the stall phenomenon does not occur until this angle of attack. A more enhanced lift coefficient is achieved compared to the baseline airfoil.

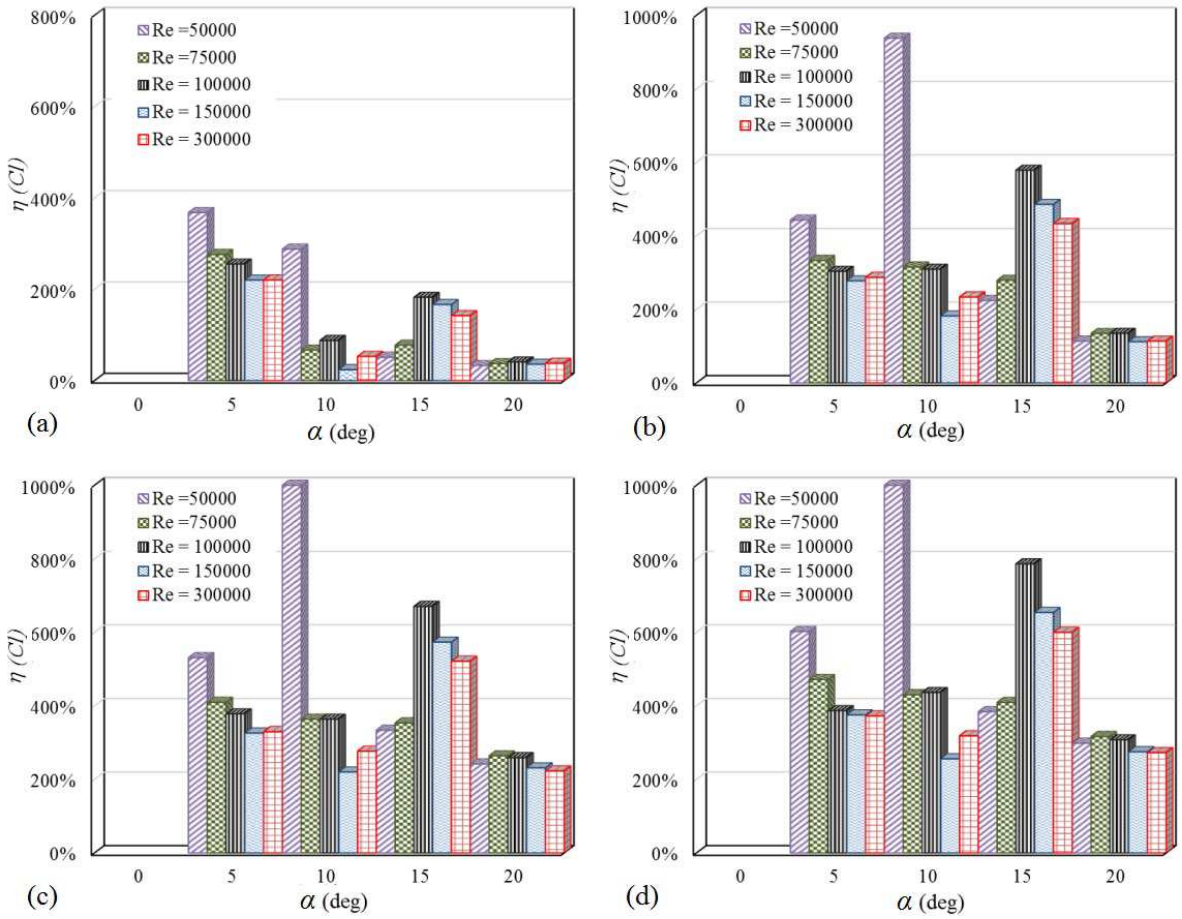

Fig. 15. Comparison of lift coefficient performance as a function of angle of attack for different Reynolds numbers at (a) C_μ =0.03, (b) C_μ =0.06, (c) C_μ =0.09, (d) C_μ =0.13.

Fig. 16 shows the performance of the drag coefficient for the CFJ at different Reynolds numbers and momentum coefficients. In most cases, by increasing the Reynolds number, the drag coefficient for CFJ airfoil rises more than that for the baseline airfoil. Furthermore, in most cases, the drag coefficient for the CFJ airfoil at Reynolds number of 50000 increases by a lower percentage.

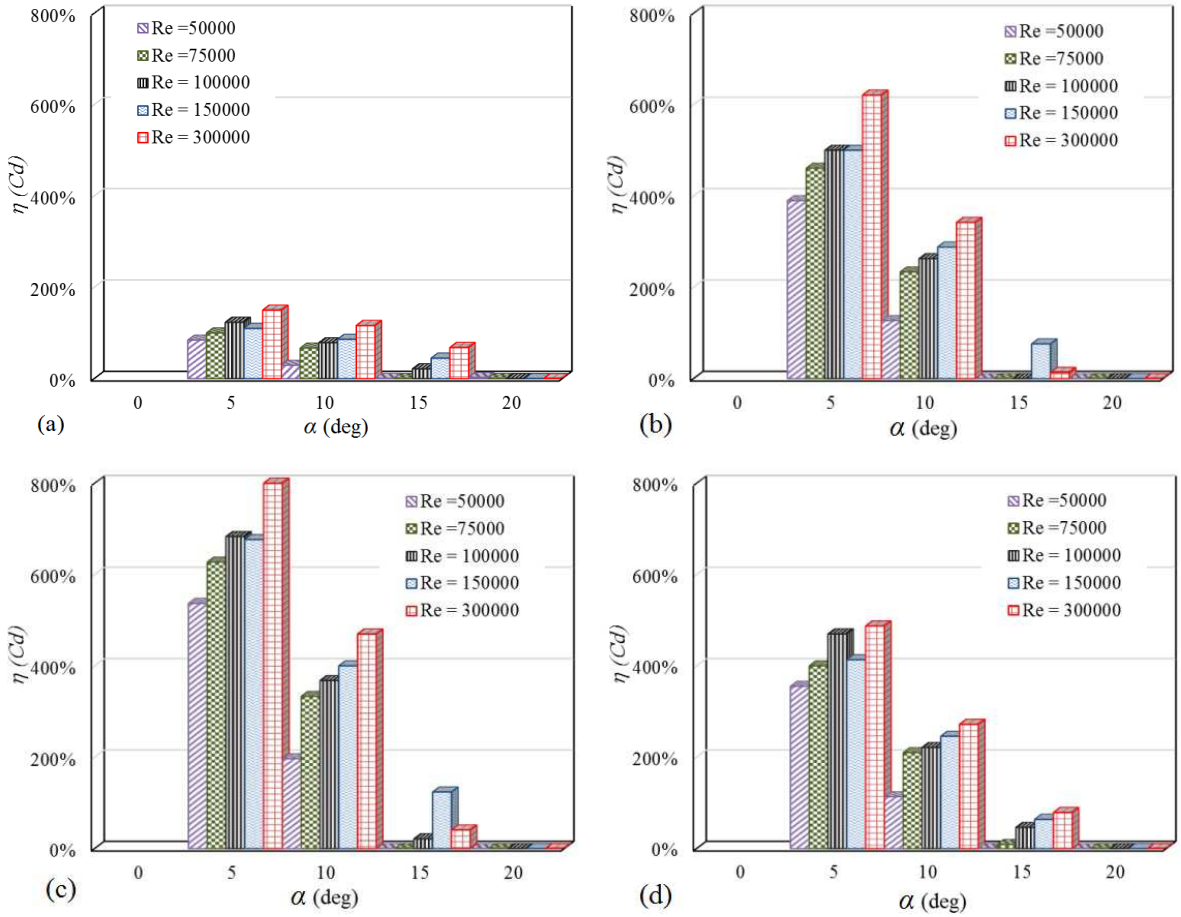

Fig. 16. Comparison of drag coefficient performance as a function of angle of attack for different Reynolds numbers at (a) C_μ =0.03, (b) C_μ =0.06, (c) C_μ =0.09, (d) C_μ =0.13.

In addition, the performance of the lift to drag coefficient for the CFJ at different Reynolds numbers and momentum coefficients are calculated as shown in Fig. 17. Compared to the baseline

airfoil, the most enhancements and the best performance of the CFJ airfoil is observed at the Reynolds number of 0.5×10^5, particularly at lower angles of attack. In other cases, the optimum lift to drag ratio for the CFJ airfoil is observed at $\alpha = 15^o$. At this angle of attack, although the drag coefficient of the CFJ airfoil is increased compared to the baseline airfoil, there is a more significant increase in the lift coefficient. Therefore, the lift to drag ratio is enhanced that can be attributed to the absence or delay of the stall phenomenon. By the occurrence of the stall phenomenon in the baseline airfoil in the vicinity of this angle, the lift and drag coefficients are substantially reduced and increased, respectively. Applying the flow control prohibits the stall, and there would be a significant enhancement within the range of the stall angles and after them.

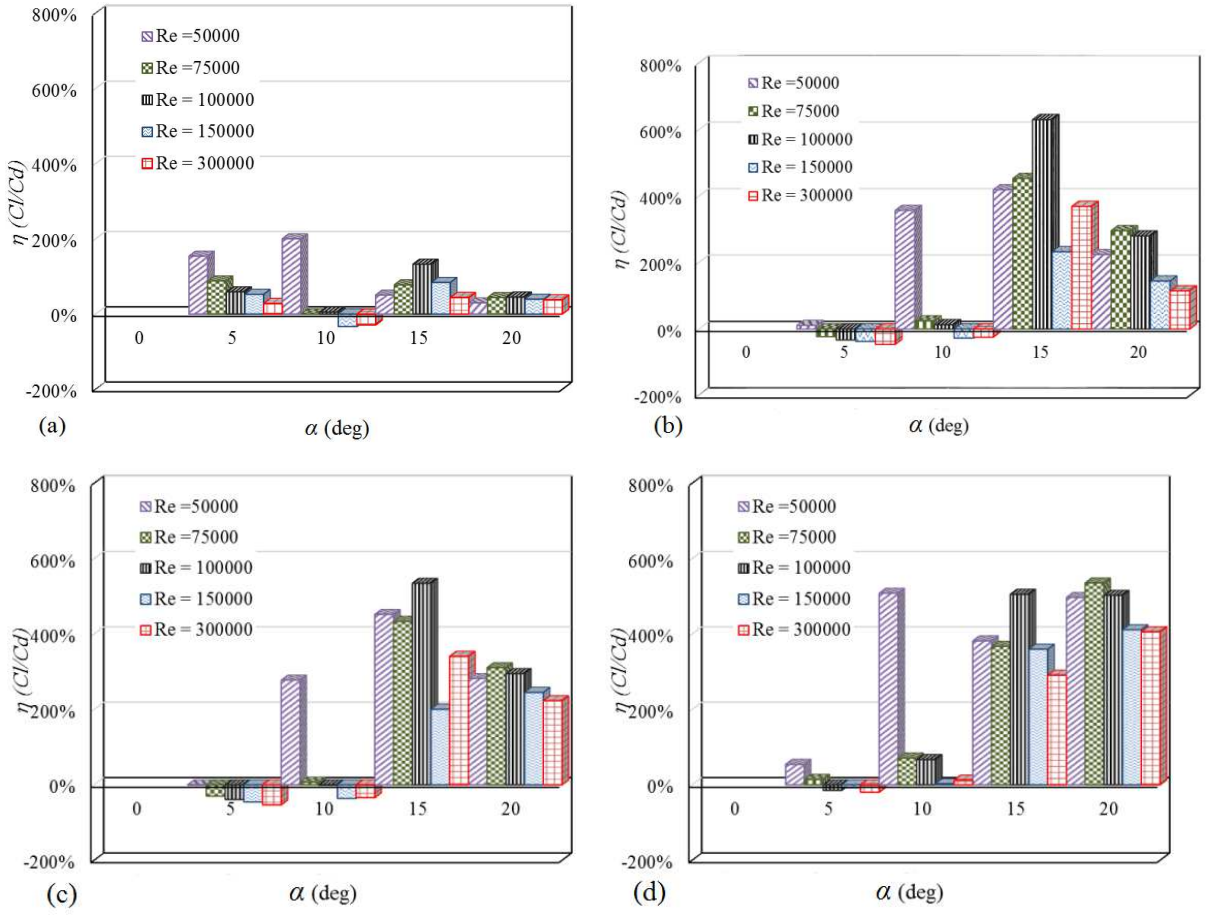

Fig. 17. Comparison of the performance of the lift to drag coefficient performance as a function of angle of attack for different Reynolds numbers at (a) C_μ =0.03, (b) C_μ =0.06, (c) C_μ =0.09, (d) C_μ =0.13.

5. Conclusions

The goal of this study is to use numerical analysis to assess the effect of an CoFlow-Jet (CFJ) on the stall and flow separation of the NACA 0024 airfoil at different Reynolds numbers ranging from 0.5×10^5 to 3×10^5. The CFJ control used two slots on the airfoil's suction surface, one for injection and one for suction. An in-house computer code based on the Reynolds-averaged Navier-Stokes equations, two-dimensional, incompressible, and unsteady with the *SST-k-ω* turbulence model, was prepared for this investigation. The solver was verified by comparing it to experimental data, which revealed a reasonably good agreement. In the present study, the performance of CFJ control was evaluated by executing CFJ control at various momentum coefficients and comparing the results to the baseline airfoil. Furthermore, the effects of this flow control on the dynamic stall at two momentum coefficients were studied. The conclusions for $Re = 1.5 \times 10^5$ are as follows:

(1) The CFJ airfoils compared to the baseline airfoil had a dramatic gain in the lift coefficients and caused the stall to occur at the higher angles of attack maintained with higher values of C_μ.

(2) Increased momentum coefficients improved the stall angles and maximum lift coefficients of all CFJ airfoils.

(3) For the angles of attack lower than the stall angles, no improvement was seen by increasing the momentum coefficient compared to the lower momentum coefficients. The trend had almost been stable.

(4) The baseline airfoil result showed the stall occurring around $\alpha = 10°$, whereas the CFJ airfoils results for $C_\mu = 0.05$ - 0.07 showed the stall occurring at $\alpha = 15°$. With further increase in the momentum coefficients, the stall angles were increased, and at $C_\mu = 0.13$, the stall did not happen until $\alpha = 30°$.

(5) by increasing the momentum coefficient, the drag coefficient increased compared to the baseline airfoil, while for higher angles, increasing the momentum coefficient led to a reduction in the flow separation zone, and consequently, the drag coefficient decreased compared to the baseline airfoil.

(6) For $\alpha \leq 15°$, C_l/C_d was maximized at $C_\mu = 0.06$.

(7) The CFJ had the highest ratio of the lift to the drag at $\alpha = 14°$ and $C_\mu = 0.06$.

(8) In the dynamic stall situation, raising the momentum coefficient from 0.05 to 0.07 resulted in a reduced lift coefficient hysteresis loop. Additionally, with $C_\mu = 0.07$, the lift coefficient curve lacked the stall feature, indicating that a stronger jet could completely manage the dynamic stall.

(9) Investigation of the Reynolds number effect indicated that by applying the CFJ, the highest enhancement in the aerodynamic coefficients was observed at the Reynolds numbers lower than 10^5. The separated flow did not reattach to the surface at the Reynolds numbers lower than 10^5, which could be yield a great reduction in the aerodynamic performance.

References

ABBASI, A. & YAZDANI, S. 2019. A Numerical Investigation of Synthetic Jet Effect on Dynamic Stall Control of Oscillating Airfoil. *Scientia Iranica,* 0**,** 0-0.

ABINAV, R., NAIR, N. R., SRAVAN, P., KUMAR, P. & NAGARAJA, S. R. 2016. CFD Analysis of Co Flow Jet Airfoil. *Indian Journal of Science and Technology,* 9.

BAK KHOSHNEVIS, A., YAZDANI, S. & SALIMIPOUR, E. 2020. Effects of CFJ flow control on aerodynamic performance of symmetric NACA airfoils. *Journal of Turbulence,* 21**,** 704-721.

CHNG, T. L., RACHMAN, A., TSAI, H. M. & ZHA, G.-C. 2009. Flow Control of an Airfoil via Injection and Suction. *Journal of Aircraft,* 46**,** 291-300.

ETHIRAJ, S. 2017. Aerodynamic performance analysis of a co-flow jet aerfoil using CFD. *International Research Journal of Engineering and Technology,* 4.

GHALAMBAZ, M., MEHRYAN, S. A. M., TAHMASEBI, A. & HAJJAR, A. 2020. Non-Newtonian phase-change heat transfer of nano-enhanced octadecane with mesoporous

silica particles in a tilted enclosure using a deformed mesh technique. *Applied Mathematical Modelling,* 85**,** 318-337.

HASHEM ZADEH, M., MEHRYAN, S. A. M., ISLAM, M. S. & GHALAMBAZ, M. 2020. Irreversibility analysis of thermally driven flow of a water-based suspension with dispersed nano-sized capsules of phase change material. *International Journal of Heat and Mass Transfer,* 155.

KHOSHNEVIS, A., YAZDANI, S. & SAIMIPOUR, E. 2020. Analysis of co-flow jet effects on airfoil at moderate Reynolds numbers. *Journal of Theoretical and Applied Mechanics,* 58**,** 685-695.

LEFEBVRE, A. & ZHA, G. 2013. Numerical Simulation of Pitching Airfoil Performance Enhancement Using Co-Flow Jet Flow Control. *31st AIAA Applied Aerodynamics Conference.*

LISSAMAN, P. B. S. 1983. Low-Reynolds-Number Airfoils. *Annual Review of Fluid Mechanics,* 15**,** 223-239.

M. SAQIBHAMEED & KAMRANAFAQ, S. 2013. Design and analysis of a straight bladed vertical axis wind turbine blade using analytical and numerical techniques. *Ocean Engineering,* 57**,** 248-255.

MUELLER, T. J. & DELAURIER, J. D. 2003. Aerodynamics Ofsmallvehicles. *Annual Review of Fluid Mechanics,* 35**,** 89-111.

OK-SOK GIM & LEE, G.-W. 2013. Flow characteristics and tip vortex formation around a NACA 0018 foil with anendplate. *Ocean Engineering,* 60**,** 28-38.

RAJAGOPALAN, R. G. & LESTARI, A. D. 2016. RK-SIMPLER: Explicit Time-Accurate Algorithm for Incompressible Flows. *AIAA Journal,* 54**,** 616-624.

SALIMIPOUR, E. 2019a. A modification of the k-kL-ω turbulence model for simulation of short and long separation bubbles. *Computers & Fluids,* 181**,** 67-76.

SALIMIPOUR, E. 2019b. A numerical study on the fluid flow and heat transfer from a horizontal circular cylinder under mixed convection. *International Journal of Heat and Mass Transfer,* 131**,** 365-374.

SALIMIPOUR, E. & SALIMIPOUR, A. 2019. Power minimization and vortex shedding elimination of a circular cylinder by moving surface mechanism. *Ocean Engineering,* 189.

SALIMIPOUR, E. & YAZDANI, S. 2020. Improvement of aerodynamic performance of an offshore wind turbine blade by moving surface mechanism. *Ocean Engineering,* 195.

SALIMIPOUR, E., YAZDANI, S. & GHALAMBAZ, M. 2021. Flow field analysis of an elliptical moving belt in transitional flow regime. *The European Physical Journal Plus,* 136.

SIDDANATHI, S. L. 2016. Application of Co-Flow Jet Concept to Aircraft Lift Increase. *International Journal of Advances in Mechanical & Automobile Engineering,* 3.

SRINATH, D. N. & MITTAL, S. 2009. Optimal airfoil shapes for low Reynolds number flows. *International Journal for Numerical Methods in Fluids,* 61**,** 355-381.

STONE, H. L. 1968. Iterative Solution of Implicit Approximations of Multidimensional Partial Differential Equations. *SIAM Journal on Numerical Analysis,* 5**,** 530-558.

VELASCO, D., LÓPEZ MEJIA, O. & LAÍN, S. 2017. Numerical simulations of active flow control with synthetic jets in a Darrieus turbine. *Renewable Energy,* 113**,** 129-140.

WELLS, A., CONELY, C., CARROLL, B., PAXTON, C., & ZHA, G. C. 2006. Velocity Field for an Airfoil with Co-Flow Jet Flow Control. *44th AIAA Aerospace Sciences Meeting and Exhibit.* Reno, Nevada.

XU, H.-Y., QIAO, C.-L. & YE, Z.-Y. 2016. Dynamic Stall Control on the Wind Turbine Airfoil via a Co-Flow Jet. *Energies,* 9.

XU, H.-Y., XING, S.-L. & YE, Z.-Y. 2015. Numerical study of the S809 airfoil aerodynamic performance using a co-flow jet active control concept. *Journal of Renewable and Sustainable Energy,* 7**,** 023131.

YARUSEVYCH, S., KAWALL, J. G. & SULLIVAN, P. E. 2006a. Airfoil Performance at Low Reynolds Numbers in the Presence of Periodic Disturbances. *Journal of Fluids Engineering,* 128**,** 587.

YARUSEVYCH, S., SULLIVAN, P. E. & KAWALL, J. G. 2006b. Coherent structures in an airfoil boundary layer and wake at low Reynolds numbers. *Physics of Fluids,* 18**,** 044101.

ZHA, G. & GAO, W. 2006. Analysis of jet effects on co-flow jet airfoil performance with integrated propulsion system. *44th AIAA Aerospace Sciences Meeting* Reno, NV, United States.

ZHA, G., GAO, W. & PAXTON, C. D. 2007. Jet Effects on Coflow Jet Airfoil Performance. *AIAA Journal,* 45**,** 1222-1231.

ZHA, G., PAXTON, C., CONLEY, C. A., WELLS, A. & CARROLL, B. F. 2006. Effect of Injection Slot Size on the Performance of Coflow Jet Airfoil. *Journal of Aircraft,* 43**,** 987-995.